European Journal of Immunology

Chronic bacterial infection activates autoreactive B cells and induces isotype switching and autoantigen-driven mutations

Sophie Jung[1,2], Jean-Nicolas Schickel[3], Aurélie Kern[4], Anne-Marie Knapp[1], Pierre Eftekhari[1], Sylvia Da Silva[1], Benoît Jaulhac[4], Robert Brink[5,6], Pauline Soulas-Sprauel[1,7,8], Jean-Louis Pasquali[1,8,9], Thierry Martin[1,8,9] and Anne-Sophie Korganow[1,8,9]

[1] CNRS UPR 3572 "Immunopathology and Therapeutic Chemistry"/ Laboratory of Excellence Medalis, Molecular and Cellular Biology Institute (IBMC), Strasbourg, France
[2] "Pôle de Médecine et de Chirurgie Bucco-Dentaires", University Hospital and Biological Sciences, Faculty of Dentistry, University of Strasbourg, Strasbourg, France
[3] Department of Immunobiology, Yale University School of Medicine, Connecticut, New Haven, CT, USA
[4] EA 7290, "Early Bacterial Virulence", Bacteriology Institute, Faculty of Medicine, University of Strasbourg, Strasbourg, France
[5] Immunology Division, Garvan Institute of Medical Research, Darlinghurst, Sydney, Australia
[6] St. Vincent's Clinical School, University of New South Wales, Darlinghurst, Sydney, Australia
[7] Faculty of Pharmacy, University of Strasbourg, Illkirch-Graffenstaden, France
[8] Department of Clinical Immunology, University Hospital, Strasbourg, France
[9] Faculty of Medicine, University of Strasbourg, Strasbourg, France

The links between infections and the development of B-cell-mediated autoimmune diseases are still unclear. In particular, it has been suggested that infection-induced stimulation of innate immune sensors can engage low affinity autoreactive B lymphocytes to mature and produce mutated IgG pathogenic autoantibodies. To test this hypothesis, we established a new knock-in mouse model in which autoreactive B cells could be committed to an affinity maturation process. We show that a chronic bacterial infection allows the activation of such B cells and the production of nonmutated IgM autoantibodies. Moreover, in the constitutive presence of their soluble antigen, some autoreactive clones are able to acquire a germinal center phenotype, to induce *Aicda* gene expression and to introduce somatic mutations in the IgG heavy chain variable region on amino acids forming direct contacts with the autoantigen. Paradoxically, only lower affinity variants are detected, which strongly suggests that higher affinity autoantibodies secreting B cells are counterselected. For the first time, we demonstrate in vivo that a noncross-reactive infectious agent can activate and induce autoreactive B cells to isotype switching and autoantigen-driven mutations, but on a nonautoimmune background, tolerance mechanisms prevent the formation of consequently dangerous autoimmunity.

Keywords: Affinity maturation · Autoreactive B cell · B-cell tolerance · Germinal center · Infection

Additional supporting information may be found in the online version of this article at the publisher's web-site

Correspondence: Prof. Anne-Sophie Korganow
e-mail: korganow@unistra.fr

Introduction

B-cell receptors (BCRs) are assembled in developing B-lymphocyte precursors via a stochastic process of joining immunoglobulin (Ig) genes. These random rearrangements inevitably result in the genesis of multiple receptors that recognize self-antigens (Ags) [1]. Despite the fact that known mechanisms of central tolerance take place in the bone marrow, many self-reactive B cells escape toward the periphery [2–5]. Most of them are the so-called natural autoimmune B cells with a mature naïve phenotype, which produce–in normal individuals—small amounts of polyreactive low affinity IgM autoantibodies (Abs) devoid of somatic mutations. A recent study performed in mice also suggests that quiescent autoreactive B cells persist in the adult repertoire and could serve as a source of pathogenic autoAbs under circumstances that still have to be defined [6].

Both genetic background and environmental factors could influence B-cell maturation in a way that favors the appearance of high affinity IgG switched autoAbs. Among known environmental factors, epidemiological studies have clearly linked infections with the occurrence of autoimmune diseases in humans and in animal models [7]. In some organ-specific autoimmune diseases, this link is attributed to molecular mimicry between pathogens and self-Ags [8–11]. The role of such mechanism in the breakdown of B-cell tolerance during systemic autoimmune diseases such as systemic lupus erythematosus (SLE) or rheumatoid arthritis seems more questionable. Studies conducted on SLE or rheumatoid arthritis patients have suggested that the disease may be induced or exacerbated by diverse bacterial (*Chlamydia pneumoniae*, *Proteus mirabilis* . . .) or viral (Parvovirus B19, Epstein Barr Virus . . .) infections [12–16]. However, SLE is associated with a wide array of autoAbs including specificities with no discernible connection to pathogens.

It is well known that bacterial or viral infections, especially chronic infections, lead to polyclonal B-cell proliferation and Ig production and that newly synthesized pathogen-specific Abs usually constitute only a small fraction of the resulting hypergammaglobulinemia [17–19]. Immune cells, including autoreactive B or T cells, express innate receptors for microbial molecules and can be directly activated through Toll-like receptors (TLRs). Substantial evidence supports a scenario in which autoreactive B cells are activated jointly by nonspecific TLR engagement and specific induction by the autoAg [20, 21].

In this context, we have previously shown that a chronic bacterial infection with *Borrelia burgdorferi* (*Bb*) [19], but not an acute viral infection with influenza virus [22], was able to break the state of immunological ignorance of autoreactive transgenic B cells, in the presence of the self-Ag, with the production of high levels of IgM autoAbs. We demonstrated that this autoAg-dependent step was induced by *Bb*-IgG immune complexes and involved stimulation of both the BCR and the MyD88-dependent TLRs pathways [19]. However, it was not possible to investigate the affinity maturation steps that could lead to production of potentially pathogenic IgG autoAbs due to the construct of this IgM transgenic model.

To gain further insight into this important issue, we have created experimental conditions in which both class switching and affinity maturation of self-reactive B cells can be followed during a bacterial infection. Our experiments demonstrate that some autoreactive B cells are activated, are able to class switch and are subject to affinity maturation leading to mutations in the H chain V region. However, in this context high affinity IgG autoAbs are not produced and paradoxically there is a selection toward lower affinity.

Results

An in vivo model for investigating self-reactive B cells with intermediate affinity

We used SW_{HEL} knock-in (ki) mice derived from the original transgenic anti-hen egg lysozyme (HEL; HyHEL10 hybridoma [23]) MD4 model [4]. In SW_{HEL} mice, the rearranged V_HDJ_H exon has been targeted to its physiologically appropriate location in the germline IgH gene, allowing normal isotype switching and somatic hypermutation (SHM) in ki B cells [24]. Although only 10–25% of the B cells express anti-HEL BCRs (due to replacement of the V_H segment by recombination of upstream V_H or V_HD elements) anti-HEL BCRs bind to wild-type (WT) HEL protein with high affinity ($K_a = 2.10^{10}$ M^{-1}). SW_{HEL} mice were previously crossed to the transgenic ML5 line producing soluble WT HEL as a neo-Ag (SW_{HEL} X ML5 model with high affinity autoreactive B cells) [24].

We selected HEL^{2X} mutant protein among a panel of previously described HEL recombinant molecules. HEL2X carries two substitutions (R73E and D101R) in the region recognized by HyHEL10 and displays intermediate affinity ($K_A = 8.10^7$ M^{-1}) for HyHEL10 [25–27]. Complementary DNA (cDNA) encoding HEL^{2X} driven by a strong ubiquitous promoter (pCAG promoter) was cloned in a transgenic vector (Supporting Information Fig. 1A). The resulting mice produce 1–10 μg/mL soluble HEL^{2X} that is recognized in vivo by anti-HEL ki B cells (Supporting Information Fig. 1B).

SW_{HEL} mice were crossed with HEL^{2X} transgenic mice and exposure to soluble HEL^{2X} induced several changes in the HEL^+ specific B-cell population. Figures 1A and B show some characteristics of HEL^+ B cells in the absence (SW_{HEL} mice) or in the presence of their autoAg (SW_{HEL} X ML5 and SW_{HEL} X HEL^{2X} mice). The percentages of splenic and lymph node (LN) HEL^+ B cells were reduced in SW_{HEL} X HEL^{2X} mice compared with SW_{HEL} mice (Supporting Information Table 1A) with a decrease in the mature population (follicular and marginal zone B cells; Fig. 1B). These self-reactive B cells also displayed an anergic phenotype characterized by downregulation of surface IgM (Fig. 1C), reduced production of IgM (Fig. 1E), or IgG anti-HEL autoAbs (Fig. 1F) and failure to upregulate CD86 under in vitro stimulation by HEL (Fig. 1D). In SW_{HEL} X ML5 mice, HEL^+ B cells were similarly regulated (Fig. 1A and B and Supporting Information Table 1A). However, autoreactive B cells proportions were significantly higher in

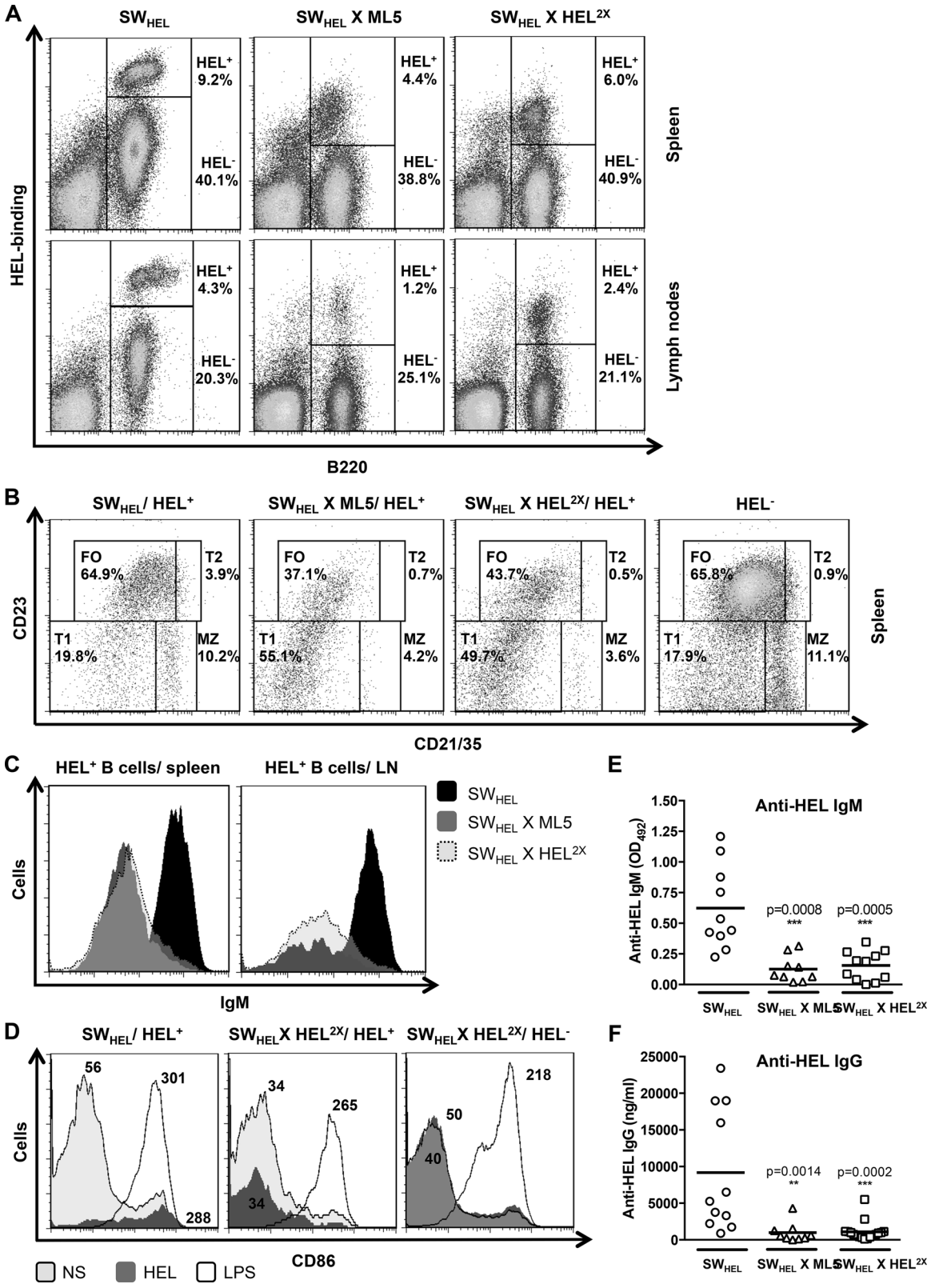

SW_{HEL} X HEL^{2X} than in SW_{HEL} X ML5 mice (Fig. 1A, $p<0.05$ in spleen and <0.001 in LN).

Despite their anergic phenotype, some autoreactive HEL^+ B cells survived in SW_{HEL} X HEL^{2X} mice and appeared relevant to study the in vivo behavior of intermediate affinity self-reactive B cells.

Borrelia burgdorferi infection partially breaks B-cell tolerance in SW_{HEL} X HEL^{2X} mice

The *Bb* spirochete, which is responsible for Lyme disease in humans, induces a chronic systemic infection characterized by recurrent bacteremia and by the invasion of many tissues in several inbred mouse strains including C57BL/6 [28–30]. It is responsible for a strong polyclonal B-cell activation via TLRs, leading to lymphoproliferation and the production of high levels of nonspecific IgM and IgG Abs [19, 31].

Four-week-old SW_{HEL} and SW_{HEL} X HEL^{2X} mice were infected with 10^5 *Bb* organisms by intradermal injection in the shaved back and analyzed 4 weeks after infection. *Bb*-specific *fla* gene was detectable in ankle joint tissues in all infected animals (Fig. 2A). Mice injected with *Bb* mounted a strong anti-*Bb* IgG response (Fig. 2B). Serum levels of HEL^{2X} protein remained similar in infected and noninfected animals (Fig. 2C).

Infection resulted in a twofold increase of LN B-cell percentage and in a 4.9 to 6.2-fold increase in LN B-cell numbers in all mice (Fig. 3B and Supporting Information Table 1B). Autoreactive HEL^+ and nonautoreactive HEL^- B-cell subsets were equally affected (Fig. 3B and C and Supporting Information Table 1B). Numbers of $CD4^+$ and $CD8^+$ T cells were also increased approximately twofold (data not shown and [32]). By contrast, we found no significant modification in the splenic B-cell populations (Supporting Information Table 1B), which was consistent with previous data showing that spleen generally harbors very low numbers of *Bb* [19, 29, 31, 32].

Bb infection was responsible for approximately a sixfold increase in total IgM and a tenfold increase in total IgG production (Fig. 3D). In vitro, both autoreactive and nonautoreactive B cells were activated by sonicated *Bb* (Fig. 4A). In SW_{HEL} mice, HEL^+ B cells were also activated by HEL Ag, simultaneous *Bb* and antigenic stimulation being synergistic (Fig. 4A).

HEL^+ B cells were able to produce anti-HEL IgM in vivo in infected SW_{HEL} and SW_{HEL} X HEL^{2X} mice (Fig. 4B). However, we did not observe a significant increase in anti-HEL IgG production in infected SW_{HEL} X HEL^{2X} animals (Fig. 4C). These data suggest that *Bb* is able to reverse partially the anergic state of self-reactive B cells.

Autoreactive B cells are able to class switch but do not differentiate properly into IgG secreting cells

To understand the lack of anti-HEL IgG secretion, we first questioned isotype switching in autoreactive B cells. We sorted LN HEL^+ B cells from *Bb* infected and noninfected animals and analyzed IgG1 and IgG2 transcripts levels. V_H Cγ1 and Cγ2b/2c transcripts could be readily visualized in infected SW_{HEL} X HEL^{2X} HEL^+ B cells compared with the near absence of γ transcripts in noninfected HEL^+ B cells (Fig. 5A). Ig expression was assessed in B-cell populations. IgG expressing B cells were clearly detected among infected SW_{HEL} X HEL^{2X} HEL^+ B cells (Fig. 5B). The transmembrane activator TACI is known to mediate class switch recombination and IgG production [33] but the expression of this receptor and of B-cell activating factor receptor (BAFF-R) did not differ between HEL^+ and HEL^- B cells in *Bb* infected mice (Supporting Information Fig. 2A). We tested in vitro the hypothesis that autoreactive B cells were intrinsically unable to differentiate into IgG secreting B cells. Purified splenic B cells were challenged with BCR-independent stimuli. HEL^- and HEL^+ B cells proliferated 4 days after stimulation (Supporting Information Fig. 3). Nonself-reactive B cells from SW_{HEL} and SW_{HEL} X HEL^{2X} donors produced

Figure 1. Phenotypic characterization of autoreactive B cells from SW_{HEL} X HEL^{2X} mice. **(A)** Flow cytometry analysis of HEL binding and B220 surface expression on splenic and LN B cells from SW_{HEL}, SW_{HEL} X ML5, and SW_{HEL} X HEL^{2X} mice. Cells were stained with anti-B220 Ab and HEL binding BCRs (HEL^+ B cells) were detected by incubating cells with saturating concentrations of HEL followed by biotinylated polyclonal rabbit anti-HEL Ab plus PE/Cy5.5-streptavidin (SA) staining. Numbers indicate the mean of HEL^+ B cells and HEL^- B-cell percentages in viable lymphocyte gate. FACS plots are representative of more than five independent experiments (SW_{HEL} $n = 11$ mice; SW_{HEL} X ML5 spleen: $n = 8$ mice, LN: $n = 10$ mice, and SW_{HEL} X HEL^{2X} $n = 16$ mice). **(B)** Flow cytometry analysis of splenic HEL^+ and HEL^- B-cell subsets from SW_{HEL}, SW_{HEL} X ML5, SW_{HEL} X HEL^+mice. Splenocytes were stained with anti-B220, anti-CD21/CD35, anti-CD23 Abs and HEL plus anti-HEL-biotin Ab plus SA. HEL^+ and HEL^- B-cell gates were determined as in Fig. 1A. Windows show Transitional 1 (T1: CD21/$CD35^{low}$ $CD23^{low}$), Transitional 2 (T2: CD21/$CD35^{high}$ $CD23^{high}$), Follicular (FO: CD21/$CD35^{int}$ $CD23^{high}$), and Marginal Zone (MZ: CD21/$CD35^{high}$ $CD23^{low}$) populations and numbers indicate the mean percentage of the displayed cells in HEL^+ and in HEL^- B-cell subsets. Data are representative of three independent experiments (SW_{HEL} $n = 6$ mice, SW_{HEL} X ML5 $n = 6$ mice, SW_{HEL} X HEL^+ $n = 8$ mice). **(C)** Flow cytometry analysis of IgM surface expression on splenic and LN HEL^+ B cells from SW_{HEL}, SW_{HEL} X ML5, and SW_{HEL} X HEL^{2X} mice. Cells were stained with anti-B220, anti-IgM Abs, and HEL plus anti-HEL-biotin Ab plus SA. Data are representative of three groups of similarly analyzed mice (SW_{HEL}: $n = 6$ mice, SW_{HEL} X ML5: $n = 6$ mice, SW_{HEL} X HEL^+: $n = 8$ mice). **(D)** Flow cytometry analysis of CD86 surface expression on SW_{HEL} and SW_{HEL} X HEL^{2X} HEL^+ B cells and on SW_{HEL} X HEL^{2X} HEL^- B cells ($B220^+$). Splenocytes were cultured for 72 h and stimulated with LPS (10 μg/mL), HEL (500 ng/mL), or medium alone. Cells were then stained with anti-B220, anti-CD86 Abs, and HEL plus anti-HEL-biotin Ab plus SA. Numbers indicate CD86 mean fluorescence intensity in one experiment. Data are representative of two independent experiments (SW_{HEL} $n = 3$, SW_{HEL} X HEL^{2X} $n = 3$). **(E)** ELISA detection of serum anti-HEL IgM in SW_{HEL} ($n = 10$ mice), SW_{HEL} X ML5 ($n = 9$ mice), and SW_{HEL} X HEL^{2X} mice ($n = 11$). Data are represented as optical density (OD) readings at 492 nm (OD_{492}) for 1:100 serum dilution. Each dot shows an individual mouse. Bars represent the mean values. The results of two-tailed Mann–Whitney test are indicated. **(F)** ELISA quantification of serum anti-HEL IgG levels (ng/mL) in SW_{HEL} ($n = 11$ mice), SW_{HEL} X ML5 ($n = 9$ mice), and SW_{HEL} X HEL^{2X} ($n = 17$ mice) mice. The concentrations were quantitated against a HyHEL5 IgG_1 standard (log-10 scale). Each dot shows an individual mouse. Bars represent the mean values. The results of two-tailed Mann–Whitney test are indicated.

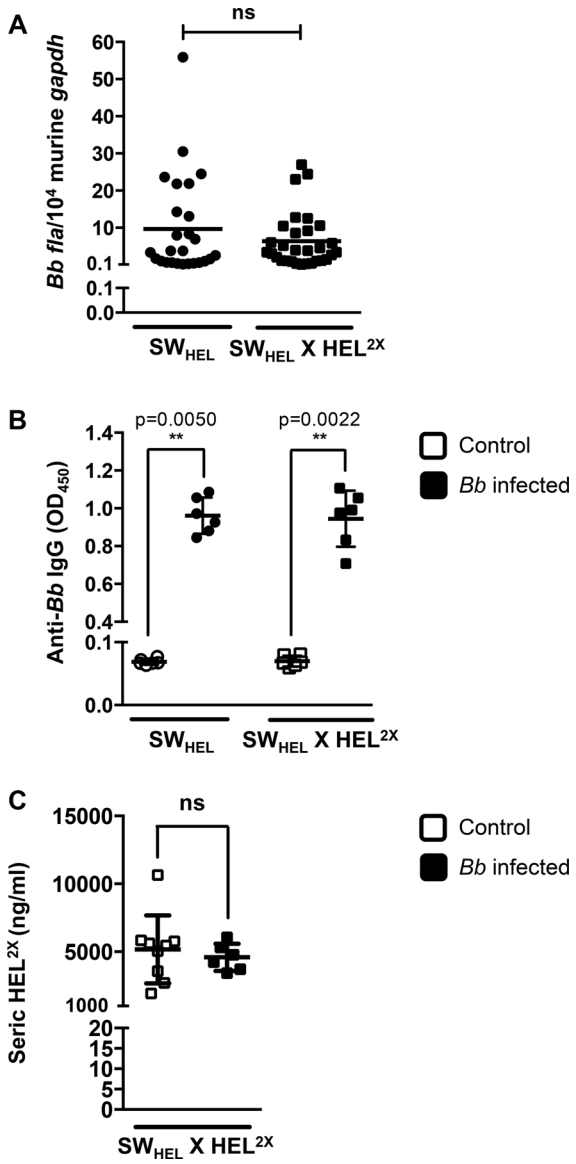

Figure 2. *Bb* infection in SW_{HEL} and in SW_{HEL} X HEL^{2X} mice. **(A)** Quantitative PCR evaluation of *Bb* DNA levels in ankle joint tissues from SW_{HEL} ($n = 26$ mice) and SW_{HEL} X HEL^{2X} ($n = 30$ mice) sacrificed 4 weeks after infection. Values represent the numbers of *Bb fla* gene copies normalized per 10^4 copies of the murine gene *gapdh*. Each dot shows an individual mouse; bold lines represent the mean values. ns: no statistical difference (Mann–Whitney test). **(B)** ELISA detection of serum anti-*Bb* IgG in infected SW_{HEL} and SW_{HEL} X HEL^{2X} mice compared with uninfected controls ($n = 6$ mice in each group). Data are represented as OD readings at 450 nm (OD_{450}) for 1:100 serum dilution. The anti-*Bb* IgG response is considered positive when OD_{450} values reach the OD of pooled uninfected mice plus 3 SD. Each dot shows an individual mouse. Data are shown as mean ±SD. The results of two-tailed Mann–Whitney test are indicated. **(C)** ELISA quantification of serum HEL^{2X} levels in infected SW_{HEL} X HEL^{2X} mice ($n = 10$ mice) compared with uninfected controls ($n = 6$ mice). Each dot shows an individual mouse; Data are shown as mean ±SD. ns: no statistical difference (Mann–Whitney test).

IgM and IgG Abs (Fig. 6A), including anti-HEL Abs in SW_{HEL} mice (Fig. 6B). However, only anti-HEL IgM were quantifiable under LPS or LPS + IL4 stimulation of SW_{HEL} X HEL^{2X} autoreactive B cells (Fig. 6B). In the same stimulating conditions, even when HEL^+ B cells numbers were adjusted, these autoreactive B cells did not secrete any anti-HEL IgG (Fig. 6C).

Taken altogether, these data demonstrate that intermediate affinity autoreactive B cells are able to survive in periphery and can be activated upon bacterial infection. They produce IgM autoAbs and are able to class-switch but not to differentiate into sufficient amounts of viable IgG secreting plasma cells, possibly due to their anergic state.

HEL^+ B cells are able to gain LN GCs and to undergo Ag-specific SHM process

In vivo, B cells can differentiate into Ig producing cells along either follicular or extrafollicular pathways. A hallmark of the follicular pathway is the formation of GCs by activated B cells where they undergo SHM followed by selection and eventually exit as high affinity long-lived IgG plasma cells or memory B cells. Upon *Bb* infection, LN autoreactive HEL^+ B cells reached a GC stage of differentiation in SW_{HEL} X HEL^{2X} mice, considering the membrane expression of GL7 and CD95 markers (Fig. 7A). Numbers of T follicular helper cells (T_{FH} cells) were similarly increased in any group of *Bb* infected mice (Supporting Information Fig. 2B) and B-cell CD40 expression appeared also comparable (Supporting Information Fig. 2A). Likewise, *Aicda* expression was induced in HEL^+ B cells from infected SW_{HEL} X HEL^{2X} mice, especially in $GL7^+$ B-cell subset (Fig. 7B). LN HEL^+ B cells were sorted (Supporting Information Fig. 6 for gating strategy) and the Ig heavy chain variable region gene was sequenced to identify SHM events. IgM V_HDJ_H rearrangements were largely unmutated (Supporting Information Tables 3A and B). However, IgG^+ HEL^+ clones from *Bb* infected SW_{HEL} X HEL^{2X} mice were enriched in mutated sequences compared with clones from *Bb* infected SW_{HEL} and from control SW_{HEL} X HEL^{2X} animals (Fig. 7C and Supporting Information Tables 2A, C–E). Most mutations were replacement substitutions located in the recognition site of HEL^{2X} protein (Fig. 7D and Supporting Information Tables 2A and E). Interestingly, these substitutions affected amino acids that interact with HEL^{2X} mutated residues [26, 27] and particularly CDR2 amino acids encoding S52, Y53 and S56 (more than 35% of sequences). They were respectively replaced by arginine (S52R), phenylalanine (Y53F), and glycine (S56G) residues in most cases (Fig. 7D, Supporting Information Tables 2A and E).

High affinity autoreactive B-cell clones are not selected in infected mice

In SW_{HEL} X HEL^{2X} model, the combination of self-Ag expression and *Bb* infection induces B-cell activation and allows the development of GCs mutated autoreactive B-cell clones.

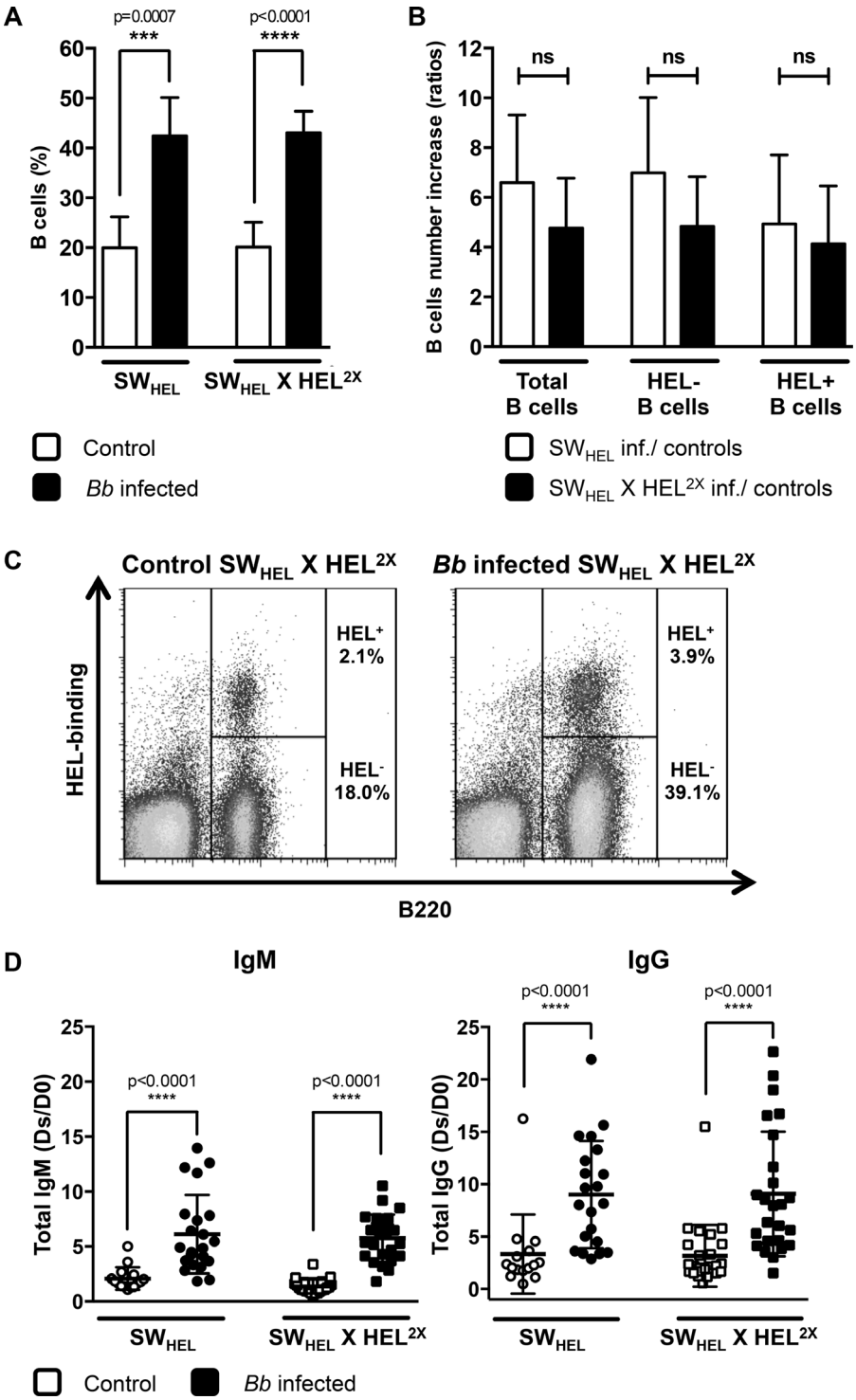

Figure 3. *Bb* infection induces LN B-cell proliferation and hypergammaglobulinemia in SW_{HEL} and SW_{HEL} X HEL^{2X} mice. **(A)** Flow cytometry analysis of LN B cells from control SW_{HEL} ($n = 7$ mice), infected SW_{HEL} ($n = 9$ mice), control SW_{HEL} X HEL^{2X} ($n = 13$ mice), and infected SW_{HEL} X HEL^{2X} ($n = 12$ mice) mice. Staining and gating strategy are described in Fig. 1A. Bars represent the mean of B-cell ($B220^+$) percentages + SD. The results of two-tailed Mann–Whitney test are indicated. **(B)** Total, HEL^- and HEL^+ B-cell number increase after *Bb* infection was determined by flow cytometry. Ratios of total, HEL^+ and HEL^- B-cell ($B220^+$) numbers were calculated for each infected animal (SW_{HEL}: $n = 9$ mice and SW_{HEL} X HEL^{2X}: $n = 12$ mice), relative to the mean of the uninfected controls of the same genotype (SW_{HEL}: $n = 7$ mice and SW_{HEL} X HEL^{2X}: $n = 13$ mice). Bars represent the means of ratios + SD for 9–12 infected mice. ns: no statistical difference (Mann–Whitney test). **(C)** Flow cytometry analysis of HEL binding and B220 surface expression from control ($n = 13$ mice) and infected ($n = 12$ mice) SW_{HEL} X HEL^{2X} mice. Staining and gating strategy are described in Fig. 1A. FACS plots are representative of more than five independent experiments. Numbers indicate the mean of HEL^+ and HEL^- B-cell percentages in viable lymphocyte gate. **(D)** ELISA quantification of serum total IgM and IgG levels in infected SW_{HEL} ($n = 22$ mice for total IgM and $n = 21$ mice for total IgG) and in infected SW_{HEL} X HEL^{2X} ($n = 24$ mice for total IgM and $n = 25$ mice for total IgG) mice compared with those in uninfected controls (SW_{HEL}: $n = 15$ mice; SW_{HEL} X HEL^{2X}: $n = 23$ mice for total IgM and $n = 26$ mice for total IgG). Values represent ratios of IgM and IgG concentrations between the day of sacrifice (Ds) and D0 in each individual infected mouse and in each individual control mouse. Each dot shows an individual mouse; bold lines represent the mean of ratios ± SD from each group of mice. The results of two-tailed Mann–Whitney test are indicated.

Previous work has suggested that SW_{HEL} GC HEL^+ B cells challenged in vivo with HEL^{2X} protein undergo affinity maturation. Extensive SHM analysis revealed that such stimulated B cells acquired in many cases a specific Ig H chain somatic mutation encoding the Y53D substitution known to increase the affinity of HyHEL10 for HEL^{2X} by at least sixfold [26]. In infected SW_{HEL} X HEL^{2X} mice, none of the amplified clones carried this mutation (Supporting Information Table 2E), arguing against an increase of autoAb affinity. Competitive ELISAs revealed that serum IgG from infected SW_{HEL} X HEL^{2X} mice did not bind HEL^{2X} more strongly than serum IgG from noninfected animals (Supporting Information Fig. 4A). To further determine whether B cells with higher affinity for HEL^{2X} could be selected, we produced several mutated recombinant HyHEL10 carrying the mutations found in IgG transcripts (Fig. 8A and Supporting Information Table 2E). We mainly focused on the most frequently observed substitutions and on the

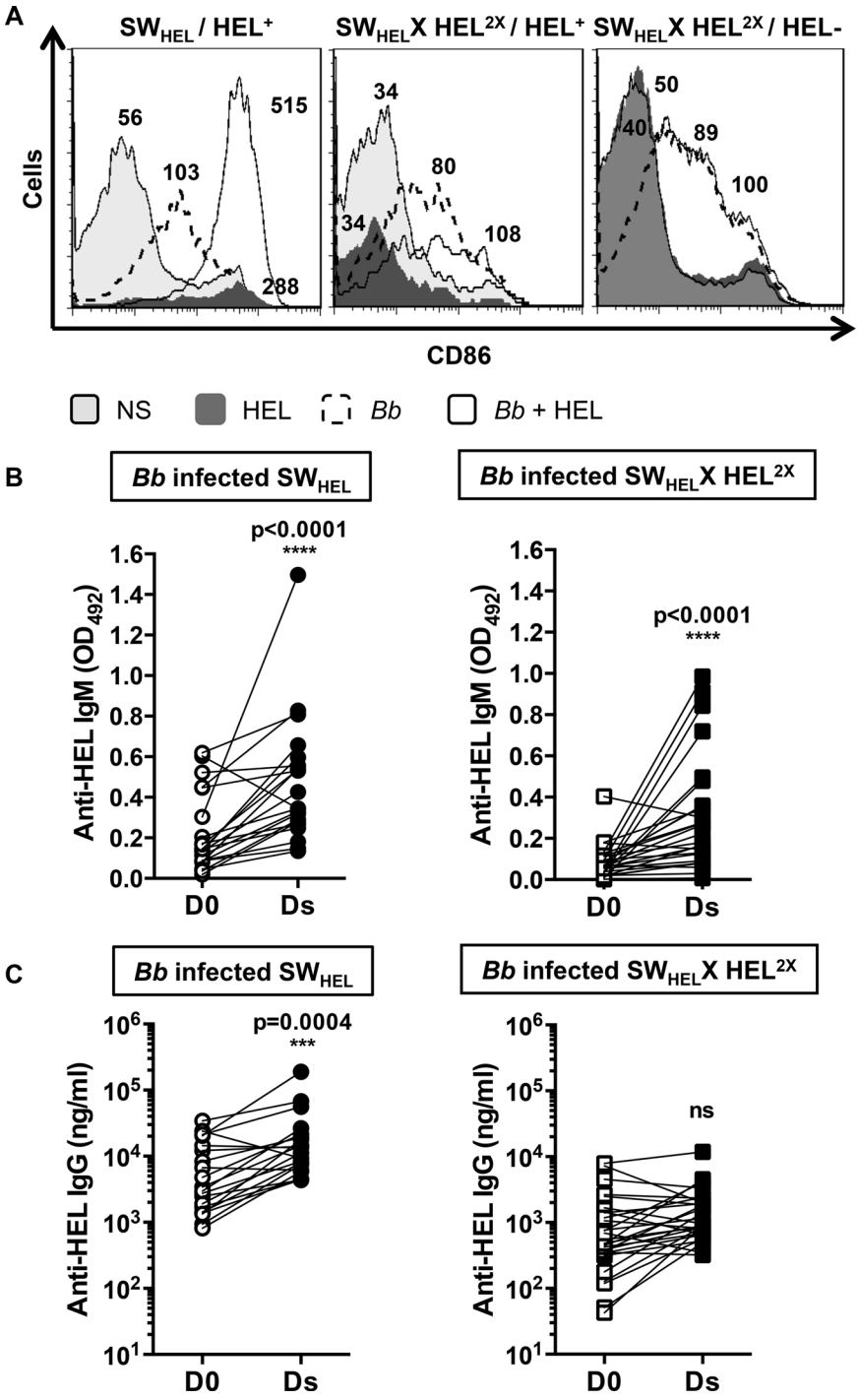

Figure 4. *Bb* infection breaks partially B-cell tolerance in SW_{HEL} X HEL^{2X} model. **(A)** Flow cytometry analysis of CD86 surface expression on HEL^+ B cells from SW_{HEL} and SW_{HEL} X HEL^{2X} mice and on HEL^- B cells from SW_{HEL} X HEL^{2X} mice. Splenocytes were cultured for 72 h and stimulated with HEL (500 ng/mL), sonicated *Bb* (10 μg/mL), sonicated *Bb* (10 μg/mL) + HEL (500 ng/mL) or medium alone. Staining was performed as in Fig. 1D. Numbers indicate CD86 mean fluorescence intensity in one experiment. Data are representative of two independent experiments (SW_{HEL} $n = 3$ mice, SW_{HEL} X HEL^{2X} $n = 3$ mice). **(B)** ELISA detection of serum anti-HEL IgM in *Bb* infected SW_{HEL} ($n = 23$ mice) and SW_{HEL} X HEL^{2X} ($n = 28$ mice) mice at day 0 (D0) and at the day of sacrifice (Ds). Data are represented as OD readings at 492 nm (OD_{492}) for 1:200 serum dilution. Each dot shows an individual mouse; lines represent the evolution in anti-HEL IgM secretion between D0 (SW_{HEL} mean value: 0.22; SW_{HEL} X HEL^{2X} mean value: 0.08) and Ds (SW_{HEL} mean value: 0.47; SW_{HEL} X HEL^{2X} mean value: 0.30) for each individual mouse. The results of two-tailed Wilcoxon matched paired tests are indicated. **(C)** ELISA quantification of serum anti-HEL IgG levels in *Bb* infected SW_{HEL} ($n = 21$ mice) and SW_{HEL} X HEL^{2X} ($n = 28$ mice) mice at day 0 (D0) and at the day of sacrifice (Ds). The concentrations were quantitated against a HyHEL5 IgG_1 standard (log-10 scale). Each dot shows an individual mouse; lines represent the evolution in anti-HEL IgG secretion between D0 (SW_{HEL} mean value: 8390 ng/mL; SW_{HEL} X HEL^{2X} mean value: 1376 ng/mL) and Ds (SW_{HEL} mean value: 25 502 ng/mL; SW_{HEL} X HEL^{2X} mean value: 1812 ng/mL) for each individual mouse. The results of two-tailed Wilcoxon matched paired tests are indicated.

residues in contact with HEL^{2X} protein (Fig. 7D and Supporting Information Table 2E). The different mutated H chains were combined with the HyHEL10-κ light chain transgene in expression vectors, as more than 98% HEL^+ B cells expressed a κ light chain (Supporting Information Fig. 5) and as κ chain carried very few mutations in infected SW_{HEL} X HEL^{2X} mice (0.53 replacement mutations per clone; Supporting Information Table 3C). By ELISA, none of the recombinant mutated HyHEL10 Abs bound HEL^{2X} with increased affinity compared with WT HyHEL10 (Fig. 8B). This was consistent with the reduced affinity of these mutated Abs for HEL^{2X} measured using surface plasmon resonance (Fig. 8C). Computer modeling suggested that the association of S52R, Y53F, and S56G substitutions was likely to affect the recognition of HEL^{2X} protein, revealing a reduced degree of freedom of HEL^{2X} R101 residue (Fig. 8D and E).

We considered the possibility that *Bb* cross-reactivity could account for these mutations. The replacement mutation rate was not significantly increased in absence of the autoAg (SW_{HEL} infected mice, Fig. 7C and Supporting Information Table 2 A–C), arguing against this hypothesis. Furthermore, none of the

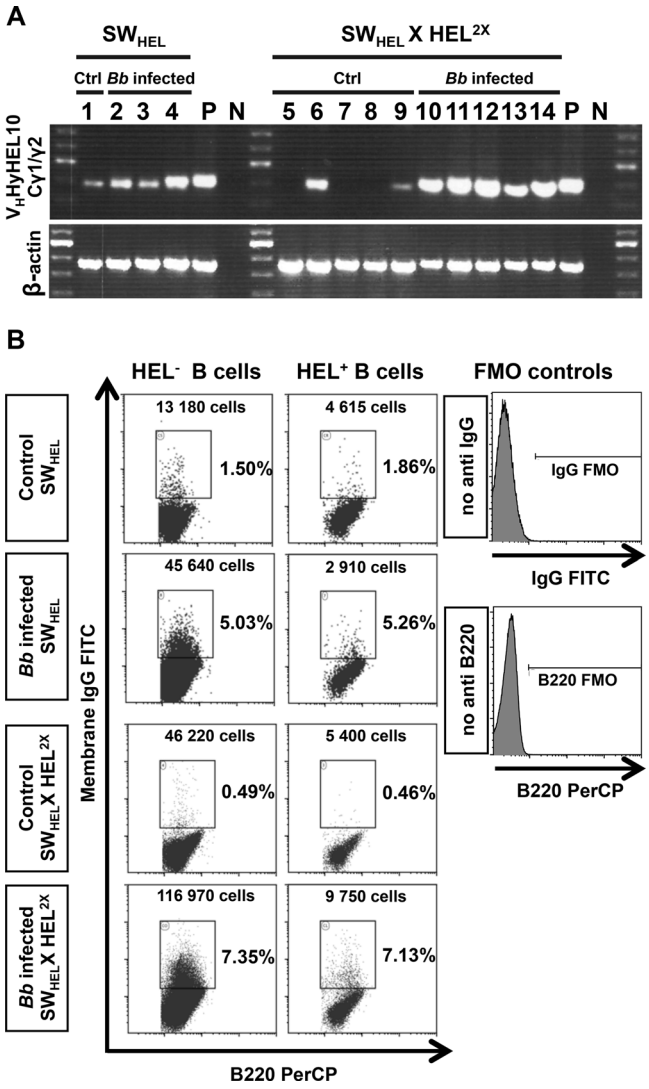

Figure 5. SW$_{HEL}$ X HEL^{2X} autoreactive B cells are able to class switch to IgG. **(A)** Semi-quantitative RT-PCR analysis of IgG$_{1\text{-}2}$ transcript expression in HEL$^+$ B cells from control (1; $n = 1$ mouse) and infected (2–4; $n = 3$ mice) SW$_{HEL}$ and from control (5–9; $n = 5$ mice) and infected (10–14; $n = 5$ mice) SW$_{HEL}$ X HEL^{2X} mice. IgG$_{1\text{-}2}$-specific amplification of the V$_H$HyHEL10 Ig variable region gene on equivalent number of HEL$^+$ FACS sorted B cells (800 cells) results in a 376 bp product. HEL$^+$ B-cell sorting strategy is detailed in the first part of Supporting Information Fig. 6. One representative gel out of 2 experiments is shown. P: positive control, N: negative control. β-actin fragment was amplified simultaneously as a control (product size: 365 bp). **(B)** Flow cytometry analysis of LN B cells expressing membrane IgG in HEL$^+$ and HEL$^-$ subsets from control and *Bb* infected SW$_{HEL}$ and SW$_{HEL}$ X HEL^{2X} mice. Cells were then stained with anti-B220-PerCP, anti-IgG-FITC Abs, and HEL plus anti–HEL-biotin Ab plus SA. Total HEL$^+$ or HEL$^-$ B-cell number and percentages of IgG$^+$ cells in HEL$^+$ or HEL$^-$ B-cell gates (B220$^+$) after dead cells exclusion (DRAQ7) in one experiment are indicated. FACS plots are representative of two independent experiments (control SW$_{HEL}$ $n = 1$ mouse, control SW$_{HEL}$ X HEL^{2X} $n = 4$ mice, *Bb* infected SW$_{HEL}$ $n = 2$ mice, *Bb* infected SW$_{HEL}$ X HEL^{2X} $n = 4$ mice). Histograms represent Fluorescence Minus One (FMO) controls.

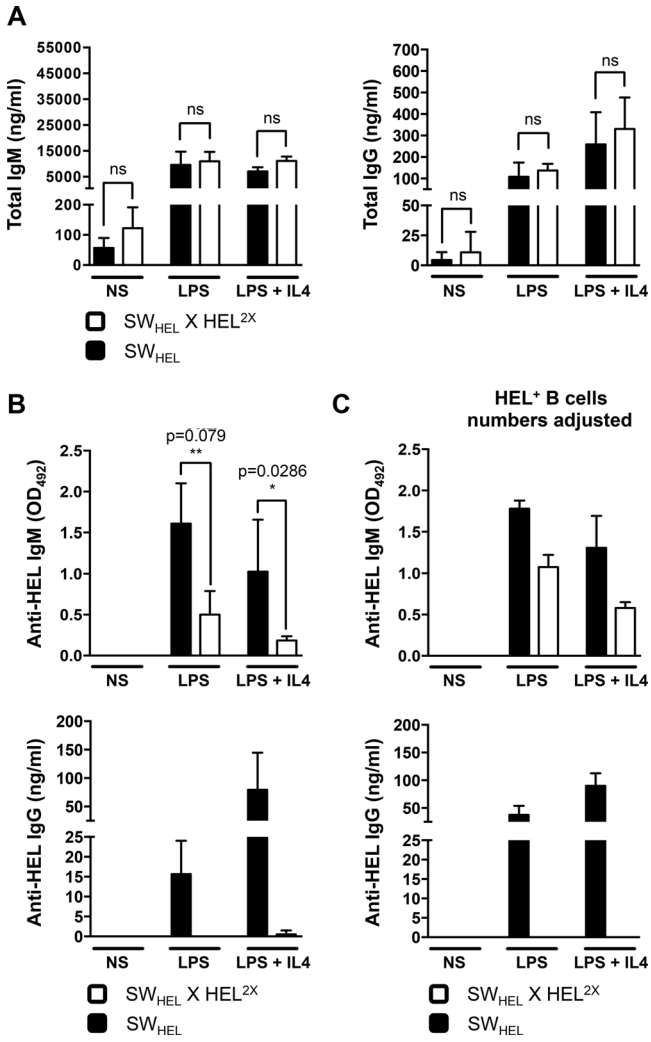

Figure 6. SW$_{HEL}$ X HEL^{2X} HEL$^+$ B cells do not differentiate into sufficient amounts of IgG$^+$ ASCs, likely due to their anergic state. **(A)** Splenic purified B cells from SW$_{HEL}$ and SW$_{HEL}$ X HEL^{2X} mice were cultured for 4 days and stimulated with LPS (25 μg/mL), LPS (25 μg/mL) + IL4 (10 ng/mL), or medium alone ($n = 4$–6 mice). ELISA quantification of total IgM and IgG levels (ng/mL) in cultures' supernatants. Each bar represents the mean value of IgM or IgG levels + SD. Data are representative of more than three experiments. ns: no statistical difference (Mann–Whitney test). **(B)** ELISA quantification of anti-HEL IgM and IgG levels in cultures' supernatants. Splenic purified B cells from SW$_{HEL}$ and SW$_{HEL}$ X HEL^{2X} mice were cultured as in Fig. 6A ($n = 4$–6 mice). Anti-HEL IgM values are represented as OD readings at 492 nm (OD$_{492}$) for 1:10 supernatant dilution. Anti-HEL IgG concentrations were quantitated (ng/mL) against a HyHEL5 IgG$_1$ standard. Each bar represents the mean value + SD. The results of two-tailed Mann–Whitney test are indicated. **(C)** Splenic purified B cells from SW$_{HEL}$ ($n = 2$ mice) and SW$_{HEL}$ X HEL^{2X} mice ($n = 2$ mice) were stimulated and cultured as in Fig. 6A and B. For SW$_{HEL}$ X HEL^{2X} mice, more splenocytes were stimulated in order to have comparable amounts of HEL$^+$ B cells as in SW$_{HEL}$ cultures (0.7×10^6 purified B cells per well for SW$_{HEL}$ mice versus 1.4×10^6 purified B cells per well for SW$_{HEL}$ X HEL^{2X} mice). ELISA quantification of anti-HEL IgM and IgG levels in cultures' supernatants. Each bar represents the mean value + SD.

monoclonal Abs (mAbs) recognized *Bb* specific Ags by ELISA (Supporting Information Fig. 4B).

Thus, while autoreactive B cells are pushed by *Bb* infection to isotype switching and enter the GCs, the process does not result in affinity maturation.

Discussion

There is a considerable amount of epidemiological data supporting a role of infections in autoimmunity [7]. It has been suggested that an infectious trigger may engage natural autoreactive B cells to produce high affinity IgG autoantibodies. A relevant hypothesis establishing the link between infections and autoimmune diseases could therefore be the progressive genesis of higher-affinity autoreactive B cells. However, the fact that most individuals are infected several times in their lifetime without developing autoimmune manifestations is at odds with this postulate. To approach this important question, we created a new in vivo model allowing a relevant study of affinity maturation process of autoreactive B cells and the comparison of ki B cells in the presence or absence of their specific self-Ag.

We focused on two related issues: whether an autoreactive B cell can be recruited into a GC reaction during infection and what the fate of such activated self-reactive cells is, if they are involved in SHM.

We show that *Bb* infection partially reverses the state of anergy of anti-HEL B cells in SW_{HEL} X HEL^{2X} model. These B cells undergo isotype switching to IgG and SHM but higher affinity clones are not selected. Furthermore, class-switched IgG autoreactive B lymphocytes do not differentiate efficiently into antibody-secreting cells (ASCs).

The first observation is that *Bb* infection can induce the activation of self-reactive B cells and the production of IgM autoAbs. IgM autoAbs are frequently and transiently detected during infections but they are usually innocuous—presumably because of their low affinities resulting from the bystander activation of so-called natural autoAbs expressing B cells. Here, our results suggest that B cells expressing autoAbs with higher affinity can also be activated. In clinical situations, this may lead to complications (leukocytoclastic vasculitis for example), that are known to occur during certain infectious diseases such as hepatitis C or endocarditis [34, 35].

A second point is that during *Bb* infection, some self-reactive B cells acquire a GC phenotype; and are able to upregulate *Aicda* gene expression and to accumulate mutations located into the recognition site of HEL^{2X} protein. GC reaction requires T-cell help [36, 37]. Although HEL-specific T cells are anergic, they are present in transgenic mice expressing soluble WT HEL [38]. HEL may also complex with *Bb* wall components due to charge interactions [39], so that *Bb*-specific T cells could participate in anti-HEL B-cell activation.

The most interesting observation is that somatic mutations—which could increase affinity for self-Ag—are not selected. Sabouri et al. recently described that SW_{HEL} X ML5 anergic B cells can be forced to gain GCs after HEL-repeated immunizations. However, the occurrence of CDR2 mutations in HEL contact surface (V51I, S52N, S56R) drives them away from self-reactivity [40]. Other studies suggested that autoreactive B cells might be able to participate in foreign Ag-driven response. Some years ago, Notidis et al. created mice expressing "dual reactivity" BCRs for the hapten Ars and nuclear autoAgs. In the context of Ars immunization, they demonstrated that negative selection by self-Ag was dominant over positive selection [41]. Our results do not support any *Bb*-positive selection. A partial help from T_{FH} cells may exist since anti-HEL B cells enter GCs and undergo SHM. This help could, however, be insufficient to allow IgG^+ GC B-cell survival [42]. Another explanation could be that soluble Ag found in the GC may engage high affinity BCRs [43]. In this view, self-reactive B cells that keep their affinity under a certain threshold could survive since soluble HEL would be less efficient to hamper them to interact with membrane-bound HEL on follicular dendritic cells.

Finally, although IgG class switching occurs in LN and autoreactive B-cell numbers increase during *B*b infection, the serum levels of anti-HEL IgG remain low. Our in vitro data suggest that isotype switched anti-HEL B cells cannot differentiate properly into ASCs. Autoreactive B cells from SW_{HEL} X HEL^{2X} mice may have an intrinsic impairment preventing the differentiation into IgG plasma cells due to chronic exposure to the autoAg, especially at the GC level. The existence of a tolerance checkpoint between the GC and plasma cell compartments has been previously suspected in other transgenic mice and in $FcRIIb^{-/-}$ mice [44–46].

This study reveals control mechanisms that are effective during chronic infection even when self-reactive B cells are activated and pushed to SHM in GCs. Thereby, we provide an explanation for the low prevalence of pathogenic IgG autoAbs in healthy individuals' sera. Introducing genetic defects that have been associated with B-cell autoimmunity into our model and exploring deeply self-reactive B cells features along with the exact role of T cells may improve the general understanding of GC reaction as well as autoimmune diseases.

Materials and methods

HEL^{2X} protein

HEL^{2X} is a recombinant version of the HEL protein that carries the D101R and R73E substitutions. HyHEL10 anti-HEL Ab binds to WT HEL with very high affinity ($K_a = 2.10^{10}\ M^{-1}$) and to HEL^{2X} protein with intermediate affinity ($K_a = 8.10^7\ M^{-1}$). HEL^{2X} retains WT HEL enzymatic activity and binds with normal affinity to the anti-HEL mAb HyHEL5, indicating normal three-dimensional folding [26, 27].

Mice

The various mouse strains used were maintained on a C57BL/6 background at the Molecular and Cellular Biology Institute

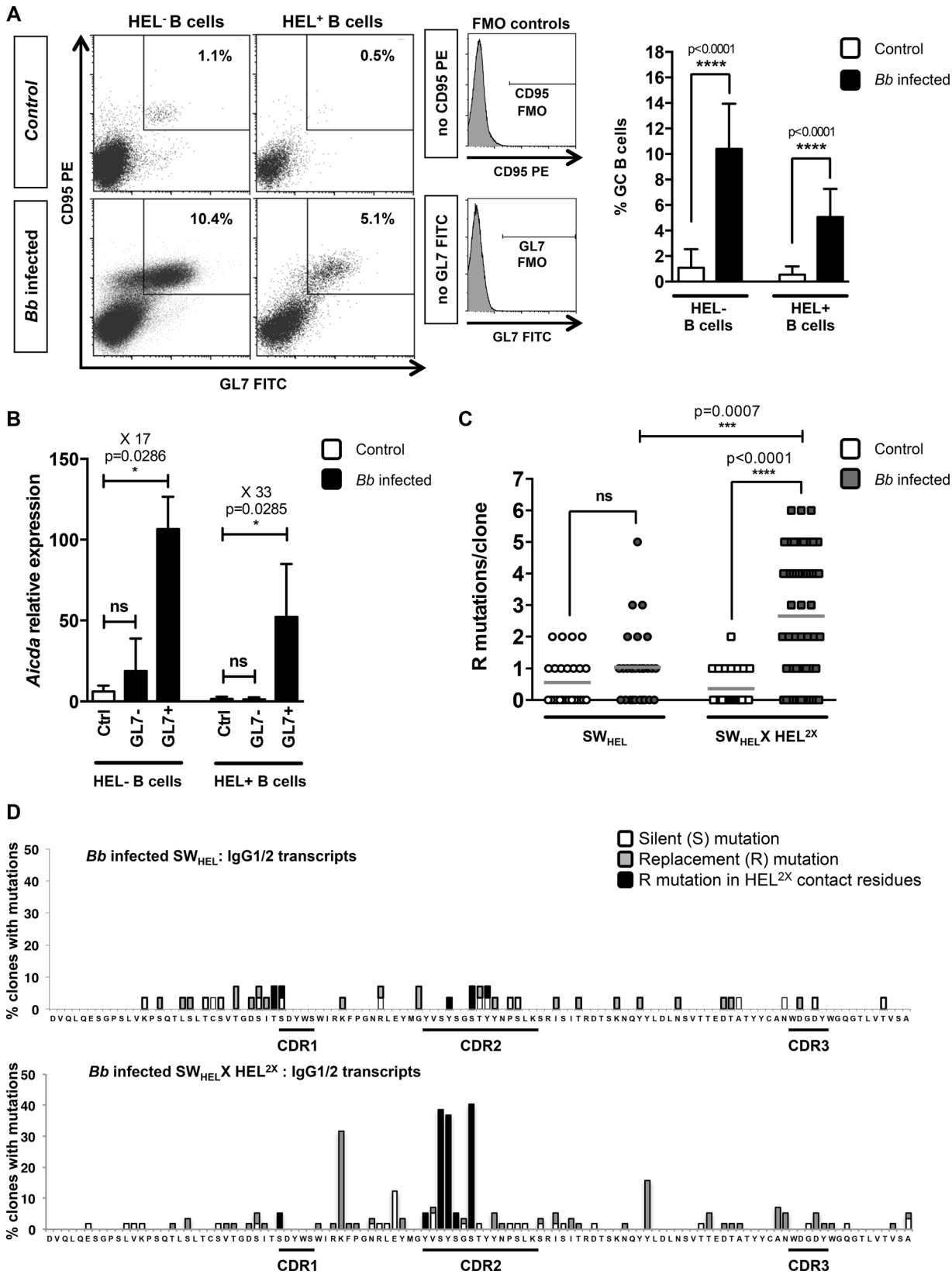

(Strasbourg). All experimental mice were heterozygous for their respective transgene. cDNA encoding HEL^{2X} mutated protein [27] was cloned in a transgenic vector with an ubiquitous strong promoter (Supporting Information Fig. 1A). Engineering of HEL^{2X} mice has been done in collaboration with the Institut Clinique de la Souris (ICS, Illkirch, France).

SW_{HEL} mice carry the rearranged V_H10DJ_H exon of HyHEL10 targeted to the J_H region of the endogenous Ig heavy-chain gene, together with a HyHEL10-κ light chain transgene [24]. SW_{HEL} mice were crossed either with the transgenic ML5 line, that express WT form of soluble HEL as a neo-self Ag under the control of the metallothionein promoter [4] or with the transgenic HEL^{2X} line, in order respectively to obtain a high affinity autoreactive model (SW_{HEL} X ML5) [24] and an intermediate affinity autoreactive model (SW_{HEL} X HEL^{2X}).

Heterozygous progeny was detected by PCR genotyping on genomic DNA and on the presence of serum HEL^{2X}. Mice were screened for the presence of their respective transgenes by PCR amplification of genomic DNA extracted from 0.5 cm of tail using Extract-N-Amp™ Tissue PCR Kit (Sigma-Aldrich).

All animal experiments were performed with the approval of the "Direction Départementale des Services Vétérinaires" (Strasbourg, France) and protocols were approved by the "Comité Régional d'Ethique en Matière d'Expérimentation Animale de Strasbourg" (CREMEAS, approval number AL/16/23/02/13). Invasive procedures were performed under inhaled anesthesia (Isoflurane, Abbott).

Borrelia burgdorferi (Bb) infection

The *Bb* sensu stricto cN40 isolate was cultivated at low passage (≤ 7) in Barbour-Stoenner-Kelly medium (BSK-H medium; Sigma-Aldrich) supplemented with 6% normal rabbit serum (Sigma-Aldrich) at 33°C. Four-week-old mice were infected with 10^5 spirochetes by intradermal injection of 100 μL in the shaved back [19, 32]. Control mice were injected with an equal volume of sterile BSK-H medium. *Bb*-inoculated mice and noninfected controls were housed in the Bacteriology Institute Animal Facility (Strasbourg, France). Arthritis was evaluated by measuring ankle joint thickness using a metric caliper (Käfer) on the thickest portion of the ankle with the joint extended at the time of injection and every week following injection. Mice were sacrificed 4 weeks after inoculation and their infectious status was assessed by quantitative PCR of the *Bb*-specific *fla* gene from DNA extracted from the right ankle joint of individual mice, as previously described [32].

Production of polyclonal rabbit anti-HEL antibody

Rabbits were injected intramuscularly with 100 μg of HEL (Sigma-Aldrich) in complete Freund's adjuvant (Life Technologies) at day 0 and with 100 μg of HEL in incomplete Freund's adjuvant (Life Technologies) at day 15, 30, and 45. Sera were collected and purified using affinity/ion exchange chromatography (DEA Affi-Gel Blue Gel, Bio-Rad). Part of the purified polyclonal anti-HEL Ab was then biotinylated (Biotine X-NHS, Calbiochem).

Flow cytometry

Cell phenotype was performed on splenic and LN lymphoid populations by four-color fluorescence analysis (dual laser FACSCalibur flow cytometer; BD Biosciences) or by eight-color fluorescence analysis (dual laser Gallios flow cytometer; Beckman Coulter) according to standard protocols. Data files were collected in the live lymphocyte gate on the basis of forward light scatter and side light scatter. When specified, dead cell exclusion was performed with DRAQ7 dye (BioStatus). Data were analyzed with FlowJo 7.5.5 (Tree Star) or Kaluza V1.2 software (Beckman Coulter).

HEL binding BCRs (HEL^+ B cells) were detected by incubating cells with saturating concentrations (200 ng/mL) of HEL

Figure 7. SW_{HEL} X HEL^{2X} HEL^+ B cells are able to gain LN GCs and express AID that regulates both isotype switching and SHM. **(A)** Flow cytometry analysis of LN GC B cells from control ($n = 11$ mice) and infected SW_{HEL} X HEL^{2X} mice ($n = 10$ mice). LN cells were stained with anti-B220, anti-T- and B-Cell Activation Marker-FITC (GL7 clone), anti-CD95-PE Abs, and HEL plus anti–HEL-biotin Ab plus SA. HEL^+ and HEL^- B-cell gates were set as in Fig. 1A. FACS plots are representative of more than five independent experiments. Numbers indicate the mean of GC B cells ($B220^+$ $GL7^+$ $CD95^+$) percentages in HEL^+ and HEL^- B-cell gates. Histograms represent Fluorescence Minus One (FMO) controls. Bars represent the mean percentages of GC B cells ($B220^+$ $GL7^+$ $CD95^+$) + SD in HEL^+ and HEL^- B-cell gates from control ($n = 11$ mice) and infected ($n = 10$ mice) SW_{HEL} X HEL^{2X} mice. The results of two-tailed Mann–Whitney test are indicated. **(B)** Quantitative real-time PCR analysis of *Aicda* expression in FACS sorted subsets from control (HEL^- and HEL^+ subsets) and infected (HEL^- $GL7^-$, HEL^- $GL7^+$, HEL^+ $GL7^-$, and HEL^+ $GL7^+$ subsets) SW_{HEL} X HEL^{2X} mice ($n =$ 4 mice). LN cells were stained with anti-B220, anti-GL7 Abs, and HEL plus anti–HEL-biotin plus SA. Cell sorting strategy is detailed in Supporting Information Fig. 6. mRNA levels were calculated using the comparative cycle threshold method and normalized to the endogenous control *Hprt1*. Each bar represents the mean of *Aicda* relative expression + SD and the results of two-tailed Mann–Whitney test are indicated. **(C)** SHM analysis was performed by cloning the anti-HEL HyHEL10 V_H10DJ_H genes after $IgG_{1\text{-}2}$-specific amplification on control ($n = 2$ mice) and infected ($n = 3$ mice) SW_{HEL} and on control ($n = 2$ mice) and infected ($n = 3$ mice) SW_{HEL} X HEL^{2X} FACS sorted HEL^+ B cells. HEL^+ B-cell sorting strategy is detailed in the first part of Supporting Information Fig. 6. HyHEL10 V_H10 gene was amplified with an FR1 and a Cγ-specific primer. Each dot represents the number of replacement mutations in an individual clone (control SW_{HEL}: 27 clones; infected SW_{HEL}: 28 clones; control SW_{HEL} X HEL^{2X}: 25 clones; infected SW_{HEL} X HEL^{2X}: 57 clones). Bold lines represent the mean of mutation frequencies in each group. The results of two-tailed Mann–Whitney test are indicated. **(D)** The sequences obtained were translated and aligned with the original HyHEL10 sequence–numbered according to Kabat et al. [48]–to determine the position of mutations. Bars represent the proportion of clones carrying silent mutations (S; white bars), replacement mutations (R; black bars), and replacement mutations in HEL^{2X} contact residues (gray bars). CDR1, CDR2, and CDR3 are indicated. The graphs show the pattern of somatic mutations in HEL^+ IgG^+ B cells from infected SW_{HEL} (28 clones) and SW_{HEL} X HEL^{2X} mice (57 clones).

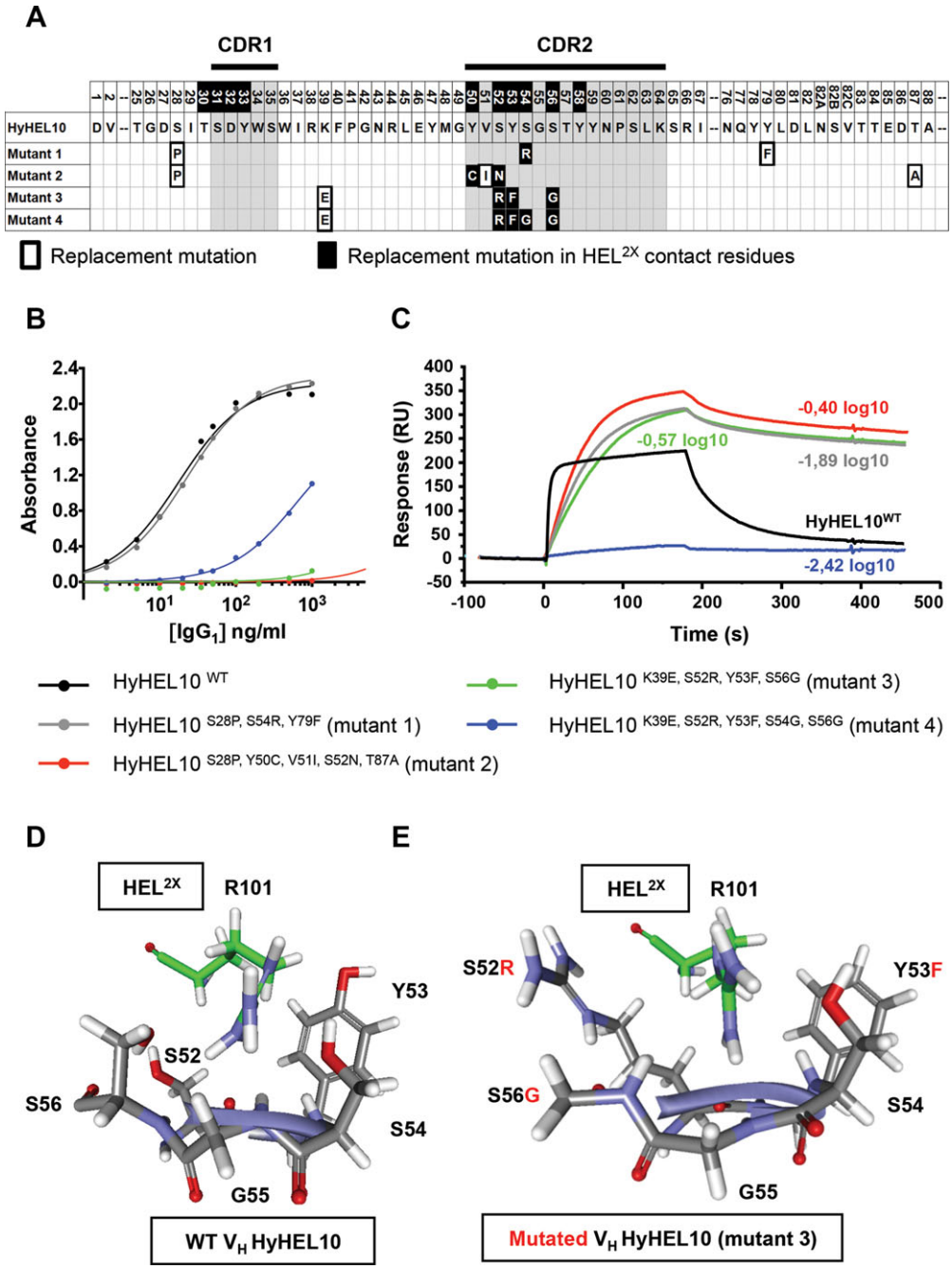

Figure 8. High affinity autoreactive clones are not selected among mutated IgG$^+$ B cells from SW_{HEL} X HEL^{2X}. Analysis of several mutated recombinant HyHEL10 IgG1 Abs designed considering the pattern of mutations found in IgG transcripts from SW_{HEL} X HEL^{2X} infected mice (see Supporting Information Table 2E). WT and mutated HyHEL10 heavy chain variable regions were cloned into an expression vector with the transgenic HyHEL10 k light chain variable region. **(A)** Amino-acid sequences from the mutated heavy chains (mutant 1–4) are shown along with the original HyHEL10 sequence [48]. Replacement mutations and replacement mutations affecting HEL^{2X} contact residues are represented. CDR1 and CDR2 regions are highlighted in gray. Amino acids in contact with HEL^{2X} protein are highlighted in black. **(B)** ELISA dose-response evaluation of the relative binding of soluble recombinant HyHEL10 WT and HyHEL10 mutated IgG1 Abs (mutants 1–4) to plate-bound HEL^{2X} (40 μg/mL). **(C)** Surface plasmon resonance analysis of the binding affinities of recombinant WT and mutated HyHEL10 Abs (mutants 1–4) for HEL^{2X}. Overlapped sensograms showing the interaction kinetics of WT and mutated HyHEL10 IgG1 Abs with HEL^{2X} (1.25e^{-9} M). The dissociation constants (K_D; M) of the interaction between mutated HyHEL10 IgG1 Abs and HEL^{2X} are expressed as the percentage difference in log from HyHEL10-HEL^{2X} K_D. **(D and E)** Tridimensional stick representations of the HyHEL10-HEL^{2X} interaction based on the crystal structure of HyHEL10 Fab-Ag complex (PDB 3D9A). Carbon (V_H HyHEL10: gray and HEL^{2X}: green), oxygen (red), nitrogen (blue), and hydrogen (white) atoms are represented. **(D)** WT V_H HyHEL10-HEL^{2X} complex showing interaction between R101 of HEL^{2X} and S52, Y53, S54, G55, and S56 residues of the HyHEL10 heavy chain. **(E)** Mutated V_H HyHEL10-HEL^{2X} complex including S52R, Y53F, and S56G substitutions in the HyHEL10 heavy chain variable region.

(Sigma-Aldrich) followed by 5 μg/mL biotinylated polyclonal rabbit anti-HEL Ab. Binding of biotinylated Ab was revealed by APC, PerCP/Cy5 (BD Biosciences), PE or PE/Cy5.5 (Southern Biotech) streptavidin (SA).

The following mAbs to murine antigens used in staining were purchased from BD Biosciences: anti-CD3e-PerCP/Cy5 (145-2C11 clone), anti-CD4-APC/Cy7 (GK1.5 clone), anti-CD21/CD35-APC (clone 7G6), anti-CD23-PE (clone B3B4), anti-CD40 APC (3/23 clone), anti-CD45R/B220-FITC and PerCP (clone RA3-6B2), anti-CD86-PE (clone GL1), anti-CD95-PE (clone Jo2), anti-CD185-biotin (CXCR5; 2G8 clone), anti-T and B Cell Activation Marker-FITC (clone GL7), PerCP/Cy5.5 and APC-Streptavidin.

Anti-IgM (μ-chain specific)-FITC and –PE, anti-CD4-PE (GK1.5 clone), anti-CD8 FITC (53-6.7 clone), anti-CD45R/B220-APC (clone RA3-6B2) and anti-CD86-APC (clone GL1) were purchased from Beckman Coulter; anti-CD267-APC (TACI; ebio8F10-3 clone), anti-CD268-FITC (BAFF Receptor; eBio7H22-E16 clone) and anti-CD279-FITC (PD-1; J43 clone) from eBioscience; anti-IgG (Fcγ-specific)-FITC from Jackson Immunoresearch; PE and PE/Cy5.5-Streptavidin from Southern Biotech.

ELISAs

Blood samples were collected before the injection of *Bb* inoculum or BSK-H medium and at the day of sacrifice. Sera were obtained by centrifugation (10 min, 10 000 rpm) of blood samples and stored at -20°C until ELISA analysis. Total IgM and IgG levels were measured as previously described [47].

For ELISA detection of the binding of murine serum Abs or HyHEL10 chimeric mAbs to HEL and HEL^{2X} protein, 96-well polystyrene plates (Nunc) were coated respectively with HEL (50 μg/mL; Sigma) or HEL^{2X} (40 μg/mL) for 2 h, blocked with 1% BSA/PBS for 30 min and then incubated with serial dilutions of sera or mAbs for 2 h at 37°C. Horseradish peroxidase-conjugated anti-mouse IgM and IgG (for murine serum anti-HEL Abs detection) or anti-human IgG (for HyHEL10 chimeric mAbs testing) were used to detect bound Abs (Jackson ImmunoResearch). They were visualized with OPD (Sigma-Aldrich) and absorbance at 492 nm was read. The concentration of serum anti-HEL IgG was evaluated by comparison with a standard curve using purified HyHEL5 monoclonal Ab. Anti-HEL IgM production was evaluated by comparison of optical density (OD) measurements at 492 nm (OD_{492}) for a 1:100 or a 1:200 dilution of the sera and for a 1:10 dilution of culture supernatants.

To detect murine serum anti-*Bb* IgG or to test HyHEL10 chimeric mAbs reactivity against *Bb*, plates were coated with 15 μg/mL *Bb* lysates. They were incubated with serial dilutions of sera or mAbs and revealed with horseradish peroxidase-coupled anti-IgG as described above. OD was read at 450 nm (OD_{450}).

Competitive inhibition ELISA was performed on sera to assess the relative affinities for HEL^{2X} of serum anti-HEL IgG. ELISA plates were coated with 40 μg/mL purified recombinant HEL^{2X} for 2 h and serial dilutions of sera were incubated with increasing dilutions of HEL^{2X}. Nonlinear regression was performed using Graph Pad Prism 5.0 software to find the curve-fit.

In vitro stimulation

In vitro experiments were performed in B-cell stimulating containing RPMI 1640® (Lonza) supplemented with 10% fetal calf serum (PAN Biotech), 100 μg/mL streptomycin (Gibco), 100 U/mL penicillin (Gibco), 50 μM 2-mercaptoethanol (Gibco), 10 mM HEPES, and 1 mM sodium pyruvate (Lonza). For proliferation analysis, purified B cells were labeled with 5 μM CFSE (CFDA SE Cell Tracer, Invitrogen) before the stimulation. B-cell activation (CD86 expression) was measured by stimulating fresh splenocytes during 72 h with LPS (Sigma), HEL (Sigma), or sonicated *Bb* (10 μg/mL) in the presence or absence of HEL. Plasma cell differentiation was determined on purified splenic B cells. They were activated for 4 days with LPS alone (Sigma) or in conjunction with recombinant murine IL-4 (Sigma).

SHM analysis

HEL^+ and HEL^- B cells were sorted on an FACSAria II flow cytometer (BD Biosciences). DAPI was used for dead cells exclusion. Cell sorting strategy is shown in Supporting Information Fig. 6. The HyHEL10 V_H10 IgH heavy chain variable region gene was amplified with a primer recognizing the first framework-coding region (GTGCAGCTTCAGGAGTCAG) and a Cμ or a Cγ1γ2aγ2b-specific primer. The primary PCR product was further amplified by semi-nested PCR with a nested primer (GCTTCAGGAGTCAGGACCTAG) and the same Cμ or Cγ1γ2aγ2b-specific primer. PCR amplification of HyHEL10 V_K10-K light chain variable region gene was performed with a primer recognizing the first framework region (GATATTGTGCTAACTCAGTCTCCAGCC) and a primer specific for the anti-HEL K light chain constant region (GGAAGATGGATACAGTTGGTGCAG). HyHEL10 heavy and light chain variable region genes were then sequenced by GATC Biotech (Konstanz, Germany). Sequences were aligned with the original HyHEL10 sequences numbered according to Kabat et al. [48] using Vector NTI Advance 11 software (Invitrogen).

Quantitative real-time RT-PCR analysis

HEL^+ and HEL^- B cells were purified by FACS sorting. In SW_{HEL} X HEL^{2X} infected mice, these populations were further separated in $GL7^+$ and $GL7^-$ cells (Supporting Information Fig. 6). mRNA was purified using RNeasy Kit (QIAGEN) and cDNA was synthesized using the High Capacity Reverse-Transcription Kit (Applied Biosystems). Five nanograms of cDNA were pre-amplified with TaqMan® PreAmp Master Mix Kit in order to increase the quantity of specific cDNA targets for gene expression analysis. Quantitative real-time PCR reactions were set up on preamplified cDNA

using TaqMan® Gene Expression MasterMix (Applied Biosystems) and Assay-on-Demand probes (*Aicda*: Mm00507771_m1, *Hprt1*: Mm01318743_m1) (Applied Biosystems). Each sample was amplified in triplicate in a StepOnePlus® real-time PCR system (Applied Biosystems). mRNA levels were calculated using the comparative cycle threshold (CT) method and normalized to the expression of *Hprt1* housekeeping gene.

Production of WT and mutated HyHEL10 IgG1 chimeric mAbs and surface plasmon resonance analysis

WT and mutated HyHEL10 heavy chain variable regions were cloned into an expression vector encoding the human Igγ1 constant region. The different HyHEL10 heavy chains were then transiently expressed in HEK 293T cells along with an expression vector encoding the transgenic HyHEL10 κ light chain variable region and the human κ1 constant region. PCR reactions, cloning strategy, expression vectors, recombinant Ab expression, and purification were performed as previously described [49]. HyHEL10 heavy chain was amplified with the primers 5'AgeI V_H (CTGCAACCGGTGTACATTCCGACGTGCAGCTTCAGGAG) and 3' SalI J_H (TGCGAAGTCGACGTGCAGAGACAGTGACCAGA) and HyHEL10 κ light chain with the primers 5' AgeI Vκ (CTG CAA CCG GTG TAC ATT CTG ATA TTG TGC TAA CTC AGT C) and 3' BsiWI Jκ (GCC ACC GTA CGG CAC GTT TTA TTT CCA GCT TGG).

For surface plasmon resonance analysis, anti-human IgG (Fcγ specific, Jackson ImmunoResearch Laboratories) was immobilized on CM-5 chip using standard amine coupling on flow cell (FC) 1 to attain a target density at 4191 RU. FC3 was used as control where polyclonal anti-human Ab was at first immobilized on FC3 using the same protocol to attain a target density at 3572 RU. The latter was thereafter digested on the chip using protein kinase A (100μM) for 200 ms with flow rate of 30 μL/min. FC2 was also used as surface control by activated and deactivated using amine protocol. HyHEL10 IgG1 mutants were injected to achieve a reading of 1000 RU over all FC 1, 2, 3, and 4 at the flow rate 30μL/min. Thereafter binding of Ag was assessed by different concentrations ($1.0e^{-8}$ to $6.0e^{-10}$ M) of HEL^{2X} over all flow cells at the same flow rate. Kinetic constants at equilibrium for both K_A and K_D were determined by fitting sensorgrams to 1:1 binding with drifting baseline model using BIAevaluation 4.1 program (GE Healthcare).

In silico exploration

In silico exploration was performed based on the crystal structure of HyHEL10 Fab complexed to HEL (PDB 3D9A) using Accelrys Discover Studio 2.5 program. S52R, Y53F, and S56G substitutions were simulated on V_H HyHEL10 and confronted to HEL^{2X} after modeling of $R73_{HEL}E$ and $D101_{HEL}R$ substitutions.

Statistical analysis

Statistical significances were calculated with a nonparametric two-tailed Mann–Whitney test using GraphPad Prism 6.0 software. A Wilcoxon test was used for paired observations. A p value of <0.05 was considered statistically significant ($^{*}p<0.05$; $^{**}p<0.01$; $^{***}p<0.001$; $^{****}p<0.0001$).

Acknowledgements: We would like to thank MC. Birling (Institut Clinique de la Souris, Illkirch-Graffenstaden, France) for HEL^{2X} mouse engineering, E. Collin and C. Barthel (EA7290, Strasbourg, France) for *Bb* infections and C. Ebel (IGBMC, flow cytometry platform, Illkirch-Graffenstaden, France) for cell sorting. We also thank M. Duval, D. Lamon, D. Bock, I. Ghazouani, K. Sablon (IBMC, Strasbourg, France), S. Weishaupt, and V. Peter (Bacteriology Institute, Strasbourg, France) for providing excellent animal care.

This work has been supported by grants from the Centre National de la Recherche Scientifique (CNRS), Hôpitaux Universitaires de Strasbourg (HUS), Université de Strasbourg (UdS), and by the ANR program "Investissements d'Avenir" (ANR-11-EQPX-022). In addition, this work has been funded in part by the Laboratory of Excellence Medalis, Initiative of Excellence (IdEx), Strasbourg University, France.

Conflict of interest: The authors declare no financial or commercial conflict of interest.

References

1 **Wardemann, H., Yurasov, S., Schaefer, A., Young, J. W., Meffre, E. and Nussenzweig, M. C.**, Predominant autoantibody production by early human B cell precursors. *Science* 2003. **301**: 1374–1377.

2 **Duty, J. A., Szodoray, P., Zheng, N.-Y., Koelsch, K. A., Zhang, Q., Swiatkowski, M., Mathias, M. et al.,** Functional anergy in a subpopulation of naive B cells from healthy humans that express autoreactive immunoglobulin receptors. *J. Exp. Med.* 2009. **206**: 139–151.

3 **Goodnow, C. C.**, Transgenic mice and analysis of B-cell tolerance. *Annu. Rev. Immunol.* 1992. **10**: 489–518.

4 **Goodnow, C. C., Crosbie, J., Adelstein, S., Lavoie, T. B., Smith-Gill, S. J., Brink, R. A., Pritchard-Briscoe, H. et al.,** Altered immunoglobulin expression and functional silencing of self-reactive B lymphocytes in transgenic mice. *Nature* 1988. **334**: 676–682.

5 **Goodnow, C. C., Crosbie, J., Jorgensen, H., Brink, R. A. and Basten, A.**, Induction of self-tolerance in mature peripheral B lymphocytes. *Nature* 1989. **342**: 385–391.

6 **Zikherman, J., Parameswaran, R. and Weiss, A.**, Endogenous antigen tunes the responsiveness of naive B cells but not T cells. *Nature* 2012. **489**: 160–164.

7 **Kivity, S., Agmon-Levin, N., Blank, M. and Shoenfeld, Y.**, Infections and autoimmunity–friends or foes? *Trends Immunol.* 2009. **30**: 409–414.

8 **Ang, C. W., Jacobs, B. C. and Laman, J. D.**, The Guillain-Barré syndrome: a true case of molecular mimicry. *Trends Immunol.* 2004. **25**: 61–66.

9 **Cunningham, M. W., Antone, S. M., Gulizia, J. M., McManus, B. M., Fischetti, V. A. and Gauntt, C. J.**, Cytotoxic and viral neutralizing antibodies crossreact with streptococcal M protein, enteroviruses, and human cardiac myosin. *Proc. Natl. Acad. Sci. USA* 1992. **89**: 1320–1324.

10 **Fujinami, R. S. and Oldstone, M. B.**, Amino acid homology between the encephalitogenic site of myelin basic protein and virus: mechanism for autoimmunity. *Science* 1985. **230**: 1043–1045.

11 **Zhao, Z. S., Granucci, F., Yeh, L., Schaffer, P. A. and Cantor, H.**, Molecular mimicry by herpes simplex virus-type 1: autoimmune disease after viral infection. *Science* 1998. **279**: 1344–1347.

12 **Draborg, A. H., Duus, K. and Houen, G.**, Epstein-Barr virus in systemic autoimmune diseases. *Clin. Dev. Immunol.* 2013. **2013**: 535738.

13 **Fujita, M., Hatachi, S. and Yagita, M.**, Acute Chlamydia pneumoniae infection in the pathogenesis of autoimmune diseases. *Lupus* 2009. **18**: 164–168.

14 **Lunardi, C., Tinazzi, E., Bason, C., Dolcino, M., Corrocher, R. and Puccetti, A.**, Human parvovirus B19 infection and autoimmunity. *Autoimmun. Rev.* 2008. **8**: 116–120.

15 **Münz, C., Lünemann, J. D., Getts, M. T. and Miller, S. D.**, Antiviral immune responses: triggers of or triggered by autoimmunity? *Nat. Rev. Immunol.* 2009. **9**: 246–258.

16 **Rashid, T. and Ebringer, A.**, Autoimmunity in rheumatic diseases is induced by microbial infections via crossreactivity or molecular mimicry. *Autoimmune Dis.* 2012. **2012**: 539282.

17 **Hunziker, L., Recher, M., Macpherson, A. J., Ciurea, A., Freigang, S., Hengartner, H. and Zinkernagel, R. M.**, Hypergammaglobulinemia and autoantibody induction mechanisms in viral infections. *Nat. Immunol.* 2003. **4**: 343–349.

18 **Montes, C. L., Acosta-Rodríguez, E. V., Merino, M. C., Bermejo, D. A. and Gruppi, A.**, Polyclonal B cell activation in infections: infectious agents' devilry or defense mechanism of the host? *J. Leukoc. Biol.* 2007. **82**: 1027–1032.

19 **Soulas, P., Woods, A., Jaulhac, B., Knapp, A.-M., Pasquali, J.-L., Martin, T. and Korganow, A.-S.**, Autoantigen, innate immunity, and T cells cooperate to break B cell tolerance during bacterial infection. *J. Clin. Invest.* 2005. **115**: 2257–2267.

20 **Leadbetter, E. A., Rifkin, I. R., Hohlbaum, A. M., Beaudette, B. C., Shlomchik, M. J. and Marshak-Rothstein, A.**, Chromatin-IgG complexes activate B cells by dual engagement of IgM and Toll-like receptors. *Nature.* 2002. **416**: 603–607.

21 **Marshak-Rothstein, A.**, Toll-like receptors in systemic autoimmune disease. *Nat. Rev. Immunol.* 2006. **6**: 823–835.

22 **Woods, A., Monneaux, F., Soulas-Sprauel, P., Muller, S., Martin, T., Korganow, A.-S. and Pasquali, J.-L.**, Influenza virus-induced type I interferon leads to polyclonal B-cell activation but does not break down B-cell tolerance. *J. Virol.* 2007. **81**: 12525–12534.

23 **Smith-Gill, S. J., Lavoie, T. B. and Mainhart, C. R.**, Antigenic regions defined by monoclonal antibodies correspond to structural domains of avian lysozyme. *J. Immunol. Baltim. Md 1950* 1984. **133**: 384–393.

24 **Phan, T. G., Amesbury, M., Gardam, S., Crosbie, J., Hasbold, J., Hodgkin, P. D., Basten, A. et al.,** B cell receptor-independent stimuli trigger immunoglobulin (Ig) class switch recombination and production of IgG autoantibodies by anergic self-reactive B cells. *J. Exp. Med.* 2003. **197**: 845–860.

25 **Padlan, E. A., Silverton, E. W., Sheriff, S., Cohen, G. H., Smith-Gill, S. J. and Davies, D. R.**, Structure of an antibody-antigen complex: crystal structure of the HyHEL-10 Fab-lysozyme complex. *Proc. Natl. Acad. Sci. USA* 1989. **86**: 5938–5942.

26 **Brink, R., Phan, T. G., Paus, D. and Chan, T. D.**, Visualizing the effects of antigen affinity on T-dependent B-cell differentiation. *Immunol. Cell Biol.* 2008. **86**: 31–39.

27 **Paus, D., Phan, T. G., Chan, T. D., Gardam, S., Basten, A. and Brink, R.**, Antigen recognition strength regulates the choice between extrafollicular plasma cell and germinal center B cell differentiation. *J. Exp. Med.* 2006. **203**: 1081–1091.

28 **Barthold, S. W., Beck, D. S., Hansen, G. M., Terwilliger, G. A. and Moody, K. D.**, Lyme borreliosis in selected strains and ages of laboratory mice. *J. Infect. Dis.* 1990. **162**: 133–138.

29 **Barthold, S. W., Persing, D. H., Armstrong, A. L. and Peeples, R. A.**, Kinetics of Borrelia burgdorferi dissemination and evolution of disease after intradermal inoculation of mice. *Am. J. Pathol.* 1991. **139**: 263–273.

30 **Wooten, R. M. and Weis, J. J.**, Host-pathogen interactions promoting inflammatory Lyme arthritis: use of mouse models for dissection of disease processes. *Curr. Opin. Microbiol.* 2001. **4**: 274–279.

31 **Tunev, S. S., Hastey, C. J., Hodzic, E., Feng, S., Barthold, S. W. and Baumgarth, N.**, Lymphoadenopathy during lyme borreliosis is caused by spirochete migration-induced specific B cell activation. *PLoS Pathog.* 2011. **7**: e1002066.

32 **Woods, A., Soulas-Sprauel, P., Jaulhac, B., Arditi, B., Knapp, A.-M., Pasquali, J.-L., Korganow, A.-S. et al.,** MyD88 negatively controls hypergammaglobulinemia with autoantibody production during bacterial infection. *Infect. Immun.* 2008. **76**: 1657–1667.

33 **He, B., Santamaria, R., Xu, W., Cols, M., Chen, K., Puga, I., Shan, M. et al.,** The transmembrane activator TACI triggers immunoglobulin class switching by activating B cells through the adaptor MyD88. *Nat. Immunol.* 2010. **11**: 836–845.

34 **Kapur, N., Tympanidis, P., Colville, C. and Yu, R. C.**, Long-term follow-up of a patient with cutaneous vasculitis secondary to mixed cryoglobulinaemia and hepatitis C virus. *Clin. Exp. Dermatol.* 2002. **27**: 37–39.

35 **Pöss, J., Schäfers, H.-J., Herrmann, M., von Müller, L., Böhm, M. and Kilter, H.**, Leukocytoclastic vasculitis and myocardial infarction as presenting manifestations of infective endocarditis: a case report. *Clin. Res. Cardiol. Off. J. Ger. Card. Soc.* 2010. **99**: 59–61.

36 **Pone, E. J., Lou, Z., Lam, T., Greenberg, M. L., Wang, R., Xu, Z. and Casali, P.**, B cell TLR1/2, TLR4, TLR7 and TLR9 interact in induction of class switch DNA recombination: modulation by BCR and CD40, and relevance to T-independent antibody responses. *Autoimmunity* 2014. **48**: 1–12.

37 **Ueno, H., Banchereau, J. and Vinuesa, C. G.**, Pathophysiology of T follicular helper cells in humans and mice. *Nat. Immunol.* 2015. **16**: 142–152.

38 **Yule, T. D., Basten, A. and Allen, P. M.**, Hen egg-white lysozyme-specific T cells elicited in hen egg-white lysozyme-transgenic mice retain an imprint of self-tolerance. *J. Immunol. Baltim. Md 1950* 1993. **151**: 3057–3069.

39 **Kumaran, D., Eswaramoorthy, S., Luft, B. J., Koide, S., Dunn, J. J., Lawson, C. L. and Swaminathan, S.**, Crystal structure of outer surface protein C (OspC) from the Lyme disease spirochete, Borrelia burgdorferi. *EMBO J.* 2001. **20**: 971–978.

40 **Sabouri, Z., Schofield, P., Horikawa, K., Spierings, E., Kipling, D., Randall, K. L., Langley, D. et al.,** Redemption of autoantibodies on anergic B cells

by variable-region glycosylation and mutation away from self-reactivity. *Proc. Natl. Acad. Sci. USA* 2014. **111**: E2567–E2575.

41 **Notidis, E., Heltemes, L. and Manser, T.**, Dominant, hierarchical induction of peripheral tolerance during foreign antigen-driven B cell development. *Immunity* 2002. **17**: 317–327.

42 **Shulman, Z., Gitlin, A. D., Weinstein, J. S., Lainez, B., Esplugues, E., Flavell, R. A., Craft, J. E. et al.,** Dynamic signaling by T follicular helper cells during germinal center B cell selection. *Science* 2014. **345**: 1058–1062.

43 **Chan, T. D., Wood, K., Hermes, J. R., Butt, D., Jolly, C. J., Basten, A. and Brink, R.**, Elimination of germinal-center-derived self-reactive B cells is governed by the location and concentration of self-antigen. *Immunity* 2012. **37**: 893–904.

44 **Culton, D. A., O'Conner, B. P., Conway, K. L., Diz, R., Rutan, J., Vilen, B. J. and Clarke, S. H.**, Early preplasma cells define a tolerance checkpoint for autoreactive B cells. *J. Immunol. Baltim. Md 1950*. 2006. **176**: 790–802.

45 **Tiller, T., Kofer, J., Kreschel, C., Busse, C. E., Riebel, S., Wickert, S., Oden, F. et al.,** Development of self-reactive germinal center B cells and plasma cells in autoimmune Fc gammaRIIB-deficient mice. *J. Exp. Med.* 2010. **207**: 2767–2778.

46 **Caton, A. J., Swartzentruber, J. R., Kuhl, A. L., Carding, S. R. and Stark, S. E.**, Activation and negative selection of functionally distinct subsets of antibody-secreting cells by influenza hemagglutinin as a viral and a neo-self antigen. *J. Exp. Med.* 1996. **183**: 13–26.

47 **Schickel, J.-N., Pasquali, J.-L., Soley, A., Knapp, A.-M., Decossas, M., Kern, A., Fauny, J.-D. et al.,** Carabin deficiency in B cells increases BCR-TLR9 costimulation-induced autoimmunity. *EMBO Mol. Med.* 2012. **4**: 1261–1275.

48 **Kabat, E. A., Wu, T. T., Perry, H. M. and Gottesman, K. S., Foeller, C.**, Sequences of proteins of immunological interest. 5th Edition. *Natl. Inst. Health*, Bethesda MD 1991.

49 **Tiller, T., Meffre, E., Yurasov, S., Tsuiji, M., Nussenzweig, M. C. and Wardemann, H.**, Efficient generation of monoclonal antibodies from single human B cells by single cell RT-PCR and expression vector cloning. *J. Immunol. Methods* 2008. **329**: 112–124.

Abbreviations: **Ab**: antibody · **Ag**: antigen · **ASC**: antibody-secreting cell · ***Bb***: Borrelia burgdorferi · **BCR**: B cell receptor · **FMO**: Fluorescence Minus One · **HEL**: hen egg lysozyme · **ki**: knock-in · **SA**: streptavidin · **SLE**: systemic lupus erythematosus · **SHM**: somatic hypermutation · T_{FH}: T follicular helper cells

Full correspondence: Prof. Anne-Sophie Korganow, CNRS UPR 3572 "Immunopathology and Therapeutic Chemistry", Molecular and Cellular Biology Institute (IBMC), 15 rue René Descartes, 67084 Strasbourg Cedex, FRANCE
Fax: + 33-3-88-61-06-80
e-mail: korganow@unistra.fr

Current address: Aurélie Kern, Division of Geographic Medicine and Infectious Diseases, Tufts Medical Center, Boston, MA, USA

Received: 19/5/2015
Revised: 25/8/2015
Accepted: 13/10/2015
Accepted article online: 17/10/2015

